CHAPTER 7

Computational investigation on the impact of point mutations on the N-terminal domain of SHANK3, indicating distinct synaptopathies in Autism Spectrum Disorder

Computational investigation on the impact of point mutations on the N-terminal domain of SHANK3, indicating distinct synaptopathies in Autism Spectrum Disorder

7.1. Abstract

Autism spectrum disorder (ASD) is a complex neurological condition with diverse clinical manifestations, encompassing challenges in social interaction, communication, and repetitive behaviors. ASD is characterized by genetic heterogeneity, converging on a limited set of molecular pathways. Synaptopathies are one of the common neuronal processes associated with ASD, involving altered glutamatergic that may disrupt the excitatory and inhibitory equilibrium. SHANK3 is pivotal as a scaffold protein connecting glutamate receptors to the cytoskeleton, crucial for synaptic transmission within the post-synaptic density. SHANK3 mutations are associated with a notable 1% of ASD. Due to the cost and time related to experimental polymorphism studies, in silico investigations are deemed a rational precursor. To elucidate the role of two mutations, SHANK3 P141A and SHANK3 L270M, implicated in ASD, we conducted a 200 ns molecular dynamics simulation to explore their functional and structural consequences on the SHANK3 protein. The P141A mutation significantly disrupted SHANK3 stabilization and caused a disturbance in intramolecular connections between SPN and ARR domains. The alteration affected the αCaMKII binding as one of the pivotal protein partners, whereas increased binding of α-Fodrin to its sites on the SHANK3. On the contrary, the SHANK3 L270M mutation resulted in moderate stability conformation. The findings underscore the intricate dynamics of SHANK3 mutations and their potential relevance to ASD.

7.2. Introduction

Autism spectrum disorder (ASD) is a composite heterogeneous neurodevelopmental condition frequently characterized by a broad spectrum of clinical manifestations, including impairments in social and communicative interactions alongside restricted, repetitive behaviors [1]. A myriad of genetic loci have been implicated in pathomechanisms of ASD [2]; however, they converge to a few molecular pathways that have been engaged in the neurobiology of ASD [3]. Synaptopathies are one of the

common neuronal processes associated with ASD as a result of genetic variations during early brain construction, involved altered glutamatergic and GABAergic neurotransmission that may disrupt the excitatory and inhibitory equilibrium [4]. One pivotal protein that plays a role within the post-synaptic density (a microstructure housing the neurotransmitter reception system of excitatory synapses within the brain) of glutamatergic neurons is SH3 and multiple ankyrin repeat domains 3 structure (SHANK3) [5]; it binds the cytoskeleton in neuronal cells to glutamate receptors and thereby plays crucial role neurotransmission and integrity [6]. SHANK3 is present in the cortex and hippocampus. However, it seems to be dominantly expressed in the thalamus and striatum [7], located in chromosome 22q13.33. It consists of five distinct domains as exhibited in (**Scheme 7.1**), involving the Shank/ProSAP N-terminal domain (SPN), which constitutes one of the essential domains of SHANK3. The SPN domain adopts a conformation resembling a ubiquitin-like (Ubl) domain analogous to Ras association domains; consequently, previous investigations have demonstrated that activated Ras and Rap proteins exhibit heightened affinity for the SPN domain of SHANK3 [8, 9]. A wide range of neuropsychological and neurological developmental conditions, including ASD, have been linked to SHANK3 mutations [10]. Significantly, a notable 1% of individuals diagnosed with ASD exhibit diverse mutations in the SHANK3 gene, thereby classifying it as a high-risk gene associated with ASD [5, 11]. Owji et al. (2020) discerned 29 deleterious missense variants within the SHANK3 gene, wherein mutations such as L47P, G54W, and G250D exhibited pronounced destabilizing effects. Molecular dynamics simulations were employed, revealing alterations in intramolecular interactions and heightened fluctuations in residues 1–350, particularly affecting the ARR functional domain [12]. These results underscore the significance of further research on these mutations within the context of SHANK3.

A recent investigation unveiled a novel SHANK3 missense mutation (L270M) situated within the ARR domain, observed in individuals displaying an ADHD-like phenotype. Functional analysis elucidated that this mutation resulted in the loss of δ-catenin binding and disrupted intramolecular interactions, consequently influencing neurodevelopmental pathology [13]. An experimental investigation involving two cohorts of individuals with ASD identified the P141A mutation and hypothesized that it plays a crucial role in the connection of SHANK3 to the membrane-associated cytoskeleton [13, 14]. In addition, they have demonstrated its impact on the colocalization of SHANK3 with other PSD

proteins [15] and its association with reduced induction and maturation of dendritic spines [16]. Noteworthy, the experimental polymorphism research are cost-prohibitive and time-consuming. In light of this, the computational approach to analyzing functional mutations has been thought to be a sensible strategy for comprehending the structural and functional implications of these polymorphisms and their impacts on the structure and stability of the SHANK3 protein. To this end, our study aims to investigate two mutations that have been found in ASD patients, namely P141A and L270M mutants, in comparison to SHANK3 WT using molecular dynamics (MD) simulations to assess the stability of SHANK3 WT, SHANK3 L270M and SHANK3 P141A structures by examining protein equilibrium, flexibility, compactness, and intramolecular interactions. Consequently, to gain insights into the potential effects of deleterious mutation on the protein binding sites implicated in neuronal transaction associated with ASD pathogenesis.

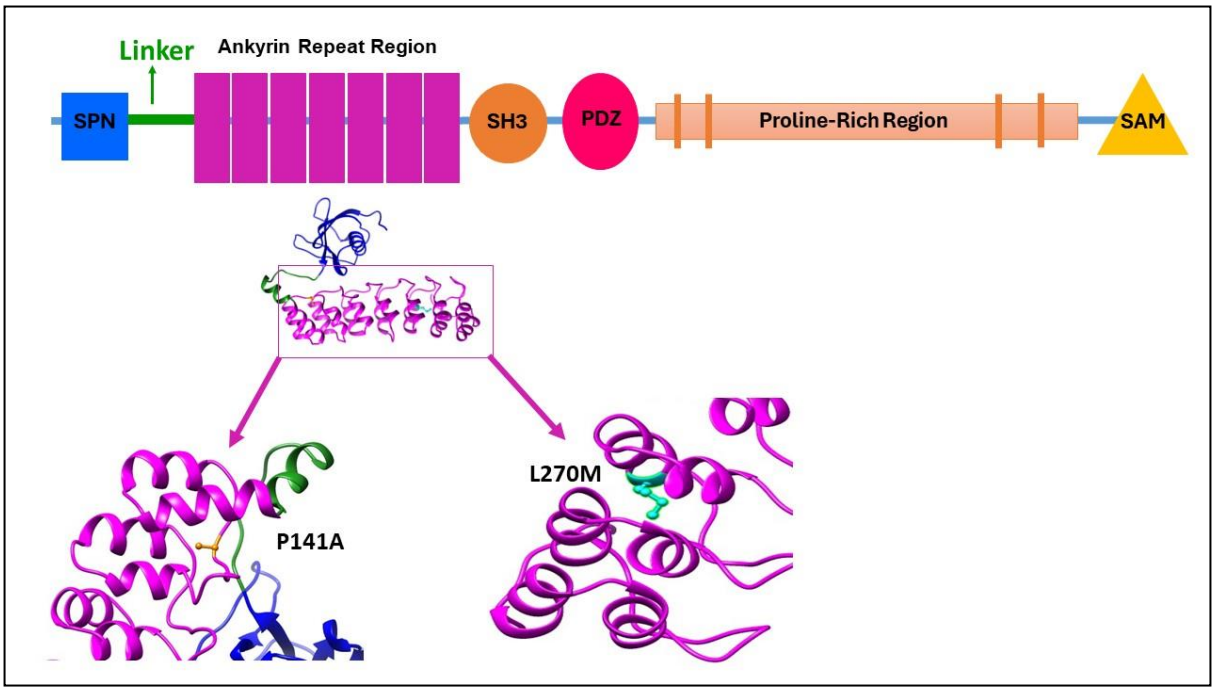

Scheme 7.1 *The domain architecture of SHANK3. The positions of the N-terminal mutations subjected to MD simulation are highlighted.*

7.3. Materials and methods

7.3.1. Preparation of initial structures

7.3.1.1. SHANK3 protein

The SHANK3 structure, PDB ID 5G4X [8], was downloaded from the RCSB Protein Data Bank [17, 18] and was utilized for molecular dynamics simulation.

7.3.1.2. Constructing the missense mutants SHANK3 L270M and SHANK3 P141A

The primary structure of the SHANK3 L270M and P141A mutants was constructed by altering the 3D structure of the scaffold protein SHANK3 WT (PDB ID: 5G4X). The Rotamer tool of the CHIMERA software [19] was applied to generate SHANK3 L270M, where Leucine was substituted with Methionine at position 270 in the SHANK3. In contrast, SHANK3 P141A was constructed by substituting Proline with Arginine at position 141 in the ARR domain of SHANK3.

7.3.2. Setup for Molecular Dynamics simulations

SHANK3 L270M, P141A, and SHANK3 WT systems were constructed for the MD simulation utilizing ff99SBildn as a force field parameter in the Leap module of the AMBER 14 software package [20]. The commonly used TIP3P water model [21] was applied as a solvent to explicitly stated SHANK3 WT and SHANK3 L270M, P141A mutant systems independently utilizing a buffer dimension of 10 Å in a periodic cubic box. The charge of the SHANK3 WT and the two SHANK3 L270M, P141A mutants structures have been neutralized by the addition of an adequate number of counter ions and afterwards, undergoing a reduction of energy to eliminate the London dispersion force.

The molecular dynamics simulation adheres to a consistent method comprising heating dynamics followed by density, equilibrium, and production dynamics. Initial structures were energy-minimized for further Molecular Dynamics procedures. The gradual heating of structures from 0 to 300 K occurred under a constant volume (NVT) situation, followed by the density approach. Equilibration was accomplished under NPT conditions (300 K and 1 atm pressure) for one nanosecond. Visualization and analysis of energy, temperature, and pressure were undertaken to ensure correct equilibration, for SHANK3 WT, and SHANK3 L270M mutant, as well as for SHANK3 P141A mutant.

Subsequently, a 200 ns MD production run for stabilized structures using the PME algorithm [22, 23] with a time step of 2 fs. A threshold of 8 Å addressed nonbonding connections, whereas electrostatic forces were managed using the PME technique. The SHAKE algorithm restricted all bonds [22] while temperature and pressure were maintained stationary via the Berendsen weak coupling algorithm over the simulation [24]. Snapshots were taken through the trajectory at intervals of 10 ns for further investigations of each structure.

The PTRAJ and CPPTRAJ modules of AmberTools 14 were applied to analyze molecular dynamics trajectories of both the SHANK3 WT and the two SHANK3 L270M, P141A mutants [22] of AmberTools 14. To evaluate the convergent behavior of our structures, the RMSDs for SHANK3 WT and the two SHANK3 L270M, P141A mutants have been analyzed, wherein the initial MD system was employed as the template for analysis.

Besides that, the three structures underwent radius gyration, hydrophobic interactions, and intramolecular distance analysis. The analysis of intra-molecular hydrogen bonds was performed for SHANK3 WT and the two SHANK3 L270M, P141A mutants according to the potential donors (HD) and acceptors (HA) of the protons. UCSF Chimera software [19] was utilized to depict the 3D structure of each system. The xmgrace plotting tools were applied to generate the plots. The monitoring of pressure, temperature, kinetic energy, total energy, and potential energy, was systematically validated throughout the simulation time for the SHANK3 WT and the two SHANK3 L270M, P141A SHANK3 mutants systems.

7.4. Results and Discussion

7.4.1. The Root Mean Square Deviation (RMSD)

RMSD analysis of atomic distances was performed over a 200 ns simulation period encompassing the SHANK3 WT protein, along with the SHANK3 L270M and P141A mutants. This analysis provided valuable insights into their conformational dynamics [25]. The RMSD of the SHANK3 WT protein exhibited a gradual increase, marked by initial fluctuations, followed by a notable transition around 3.9 Å, ultimately stabilizing towards the conclusion of the simulation (**Figure 7.1A**). Conversely, the SHANK3 L270M mutant displayed a sudden increase in RMSD with fluctuations, characterized by

intense dynamic at 3.7 Å, followed by a decrease in RMSD, then later stabilized to the end of the simulation (**Figure 7.1C**). Similarly, the SHANK3 P141A mutant exhibited an abrupt increase in RMSD, followed by fluctuations and another impulse at 4.2 Å, then a gradual increase beyond 150 ns (**Figure 7.1E**). These results suggest that the SHANK3 WT and SHANK3 L270M mutant could be slightly stable compared to the SHANK3 P141A mutant, which might have high structure flexibility. To discern the domain that contributes to these conformational changes, RMSD analyses were conducted for the three domains SPN, ARR, and Linker separately. Notably, RMSD traces restricted to the SPN and ARR domains revealed the same pattern noticed for the SHANK3 WT protein (**Figure 7.1B**). The SHANK3 L270M mutant also revealed no significant RMSD related to a specific domain (**Figure 7.1D**). In contrast, the SPN and Linker domains in the SHANK3 P141A mutant revealed distinctively increased fluctuations, suggesting their potential involvement in constitutional modifications, as exhibited in (**Figure 7.1F**).

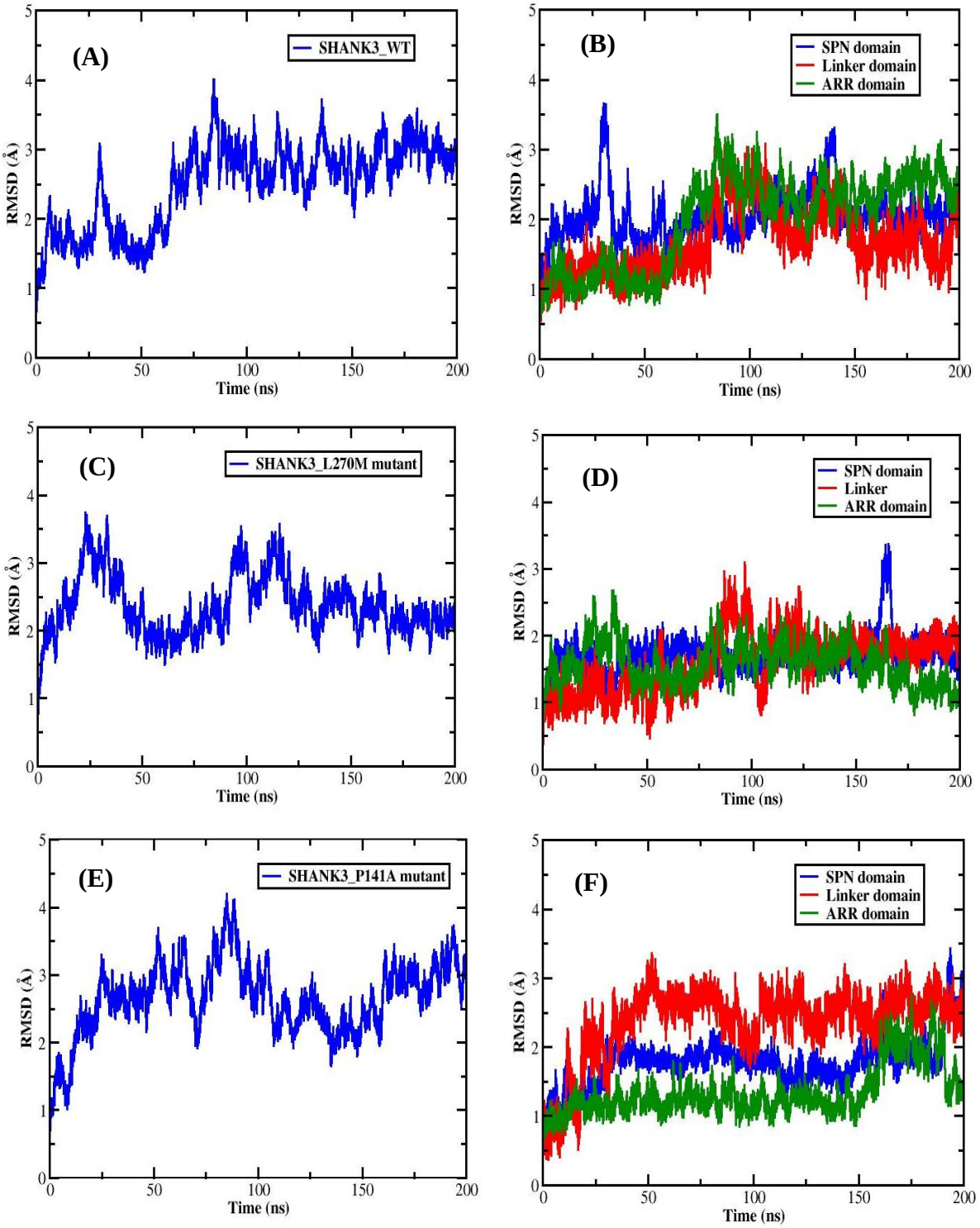

Figure 7.1 *The plot of RMSD for (**A**) SHANK3 WT protein, (**B**) Three domains in SHANK3 WT, (**C**) SHANK3 L270M mutant, (**D**) Three domains in SHANK3 L270M mutant, (**E**) SHANK3 P141A mutant, (**F**) Three domains in SHANK3 P141A mutant.*

7.4.2. The Root Mean Square Fluctuation (RMSF)

The results of RMSF demonstrated slightly increased conformational flexibility in the SHANK3 WT compared to the two mutants SHANK3 L270M and P141A (**Figures 7.2A**, **7.2C**, and **7.2E**), respectively. Noteworthy was the flexibility observed in amino acid residues corresponding to the SHANK3 SPN and Linker domains in SHANK3 WT and the two mutants, as depicted in (**Figures 7.2B**, **7.2D**, and **7.2F**). Hence, it can be inferred that the SPN and Linker domains may possess functional significance owing to their elevated RMSF values.

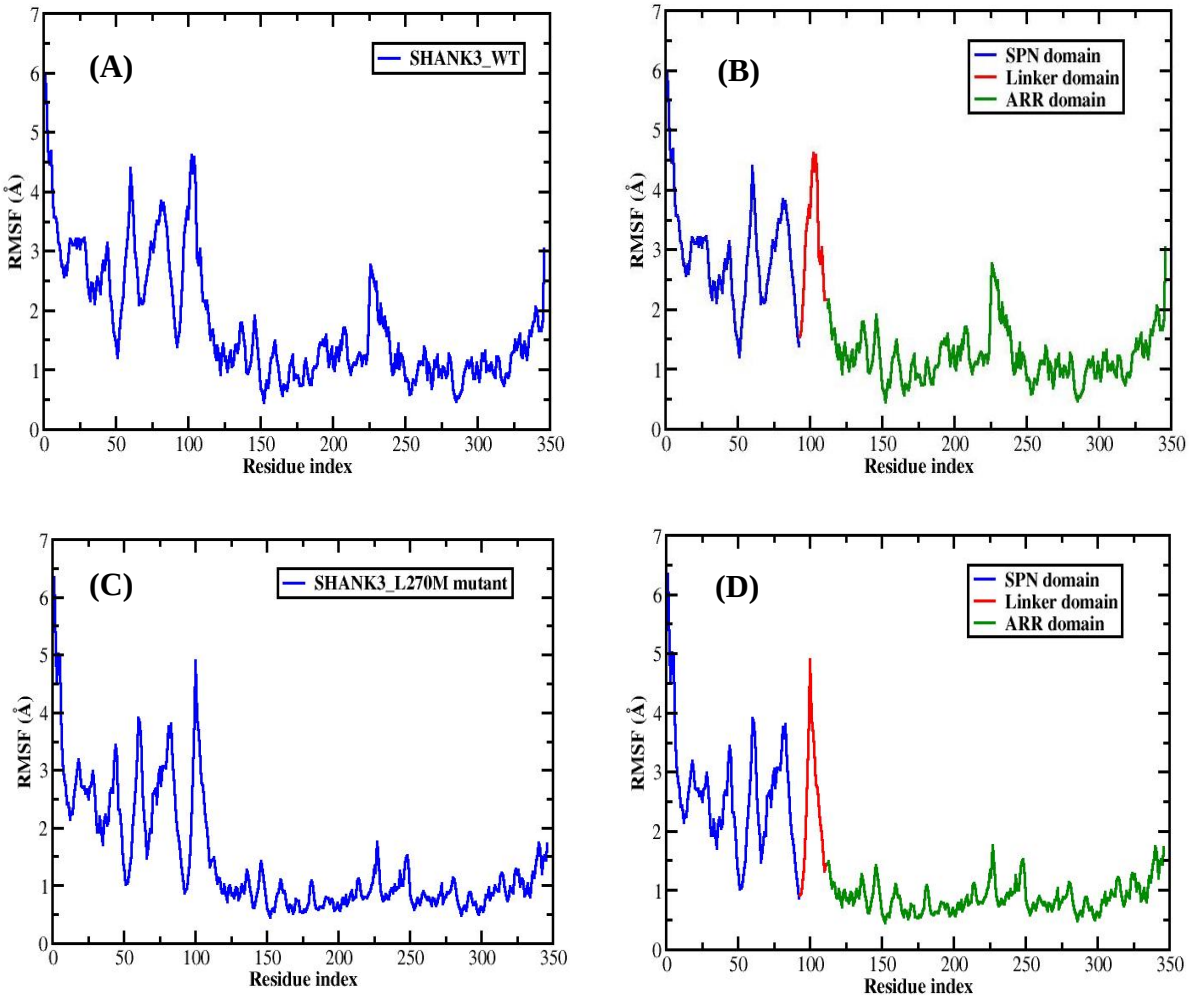

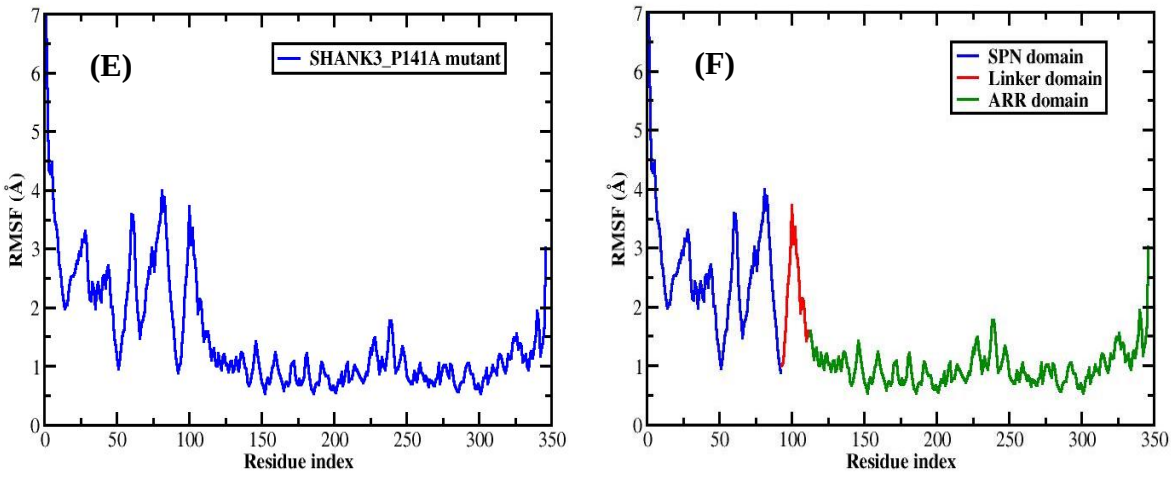

Figure 7.2 *RMSF plots for the (**A**) SHANK3 WT protein, (**B**) Three domains in SHANK3 WT, (**C**) SHANK3 L270M mutant, (**D**) Three domains in SHANK3 L270M mutant, (**E**) SHANK3 P141A mutant, (**F**) Three domains in SHANK3 P141A mutant.*

7.4.3. The Radius of Gyration (Rg) analysis

The radius of gyration (Rg) is a frequently employed metric for assessing the spatial distribution of atoms within a specific biological molecule, measured from the principal center of gravity [26]. The radius of gyration is utilized to monitor changes in structural compactness and folded over simulation time. According to the Rg plots, the SHANK3 WT protein disclosed lower values over time of the simulation of 200 ns comparison to the L270M and SHANK3 P141A mutants, as exhibited in (**Figures 7.3A**, **7.3B**, and **7.3C**, respectively). Notably, the SHANK3 P141A mutant has the highest Rg values throughout the simulation; therefore, the SHANK3 P141A mutant refers to a less compact and unfolded state. Noteworthy, the SHANK3 L270M mutation is positioned within the hydrophobic part of the ARR domain without displaying significant characteristics of an unfolding state, as the majority of the interactions within the SHANK3 N-terminal region remain preserved.

Woike et al.[13], observed a reduction in δ-catenin binding which contributed to the relatively milder ASD phenotype. Thereby, the plausible interpretation from the previous study and our findings that the SHANK3 L270M mutation subtly modifies the surface characteristics of the ARR domain in a manner incompatible with δ-catenin binding. Herein, it is worth noting that loss-of-function mutations in the CTNND2 gene that encodes δ-catenin have been linked to an ADHD phenotype [27]. Consequently, further

experimental investigations are required to elucidate the impact of the SHANK3 L270M in ASD.

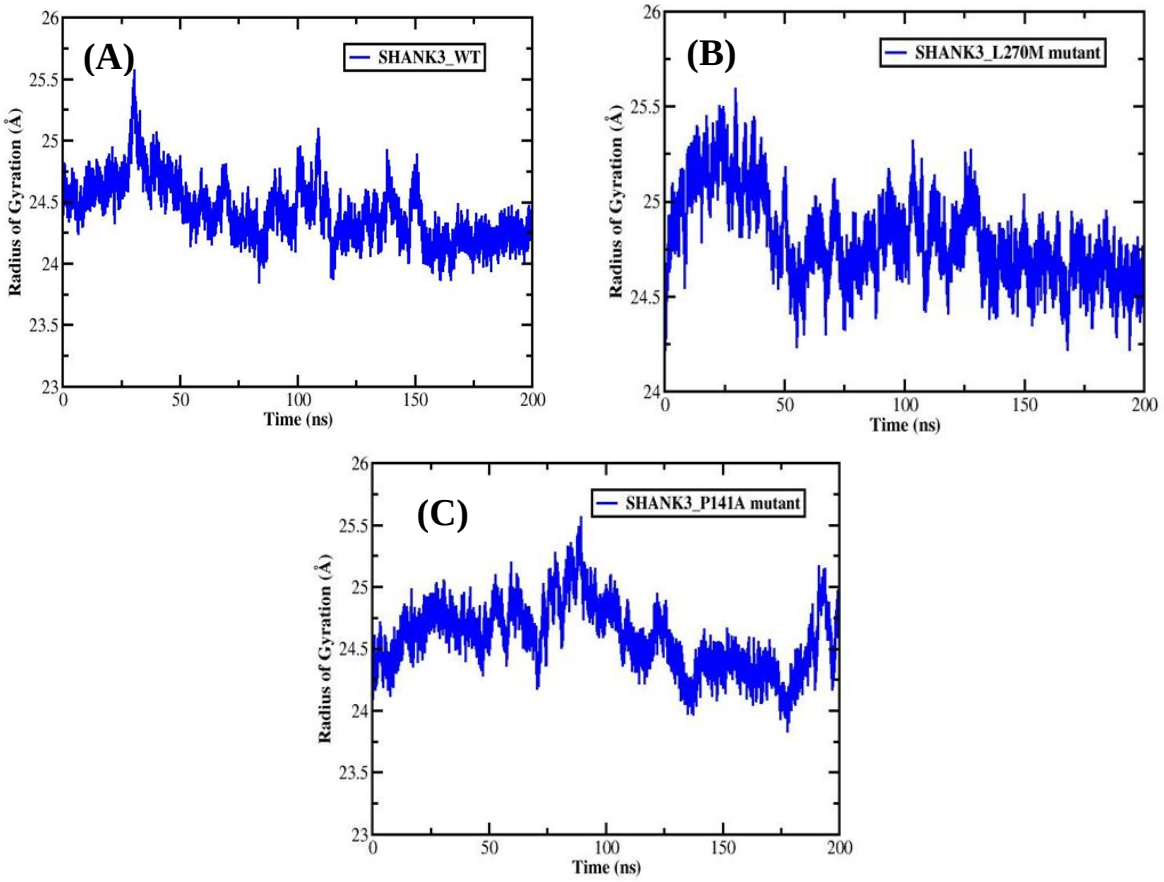

Figure 7.3 *The radius of gyration plots, (**A**) SHANK3 WT protein, (**B**) SHANK3 L270M mutant, and (**C**) SHANK3 P141A mutant. The time in the ns is on the x-axis, whereas Rg is on the y-axis.*

7.4.4. Analysis of the distance between center of mass SPN and ARR domains

The central point of mass distance between the SPN-ARR domains of SHANK3 WT and the two mutants SHANK3 L270M and P141A was assessed. The distance between SPN-ARR in the SHANK3 WT protein increased initially, followed by a sudden reduction (**Figure 7.4A**). Conversely, the SHANK3 L270M mutant exhibited an initial increase in distance, gradually decreasing to a conserved state between the two domains (**Figure 7.4B**). In contrast, the SHANK3 P141A mutant showed a continuous increase in distance, suggesting an impact on domain interactions and the potential open-up of the SPN-ARR fold over time (**Figure 7.4C**).

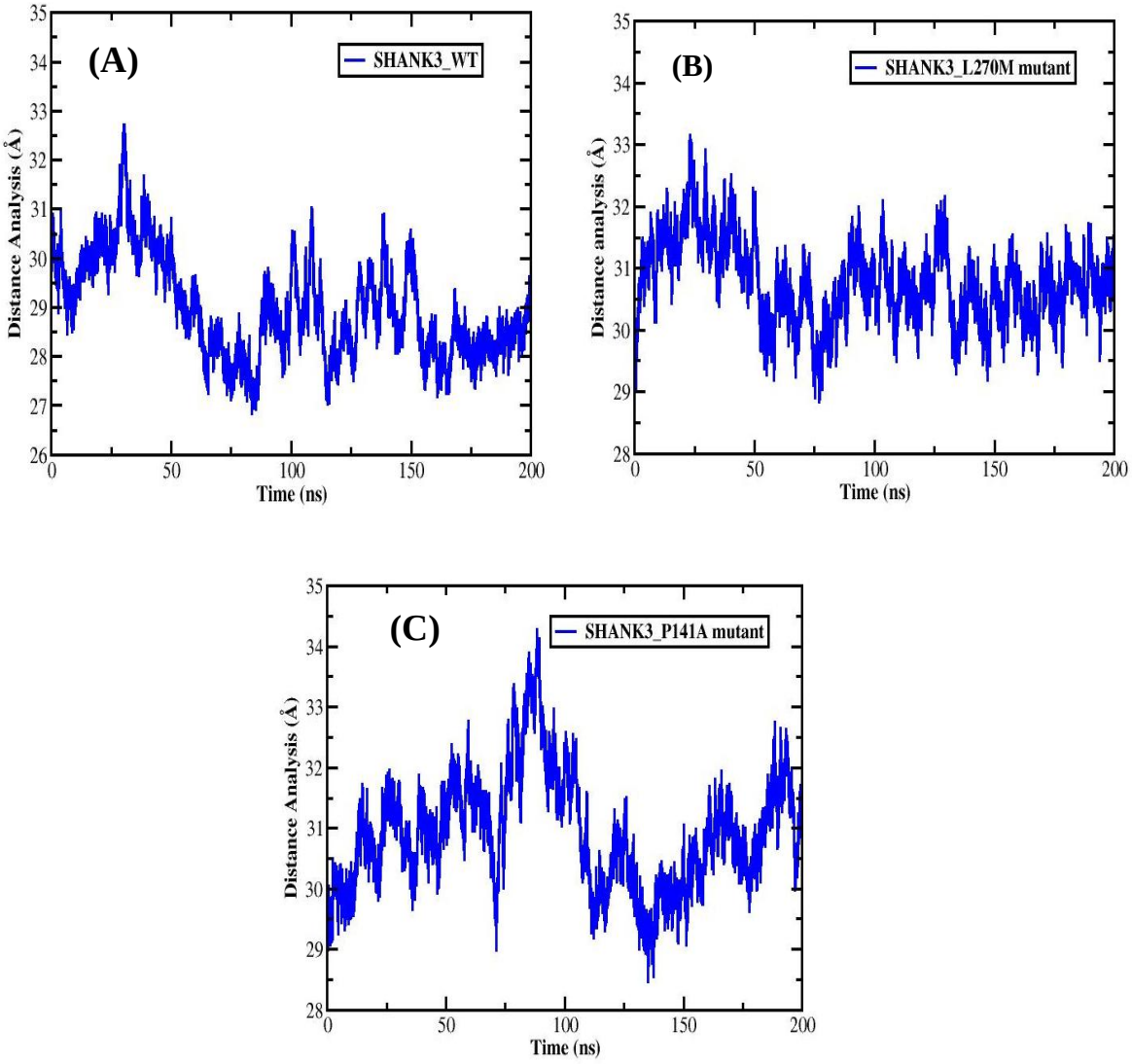

Figure 7.4 *The distance between SPN and ARR domains analysis, (**A**) SHANK3 WT protein, (**B**) SHANK3 L270M mutant, (**C**) SHANK3 P141A mutant.*

7.4.5. Intra-molecular hydrogen bond analysis

Intramolecular hydrogen bonds were quantified to assess the proximity of all-atom interactions within the SHANK3 WT protein and its two mutants, SHANK3 L270M and P141A. These intramolecular hydrogen bond contacts serve as pivotal metrics for gauging the structural compactness within the distinct domains of the SHANK3 WT protein. The results revealed an increase in intra-molecular interactions in the SHANK3 WT protein in comparison with the SHANK3 L270M and SHANK3 P141A mutants, with the lowest number of hydrogen bonds observed in the SHANK3 P141A mutant, as illustrated in (**Figures 7.5A**, **7.6A**, and **7.7A**). Similarly, the SPN domain exhibited higher disparities in the SHANK3 WT protein compared to the SHANK3 L270M and SHANK3 P141A mutants (**Figures 7.5B**, **7.6B**, and **7.7B**). Furthermore, the ARR domain displayed fewer intramolecular hydrogen bonds in the SHANK3 P141A mutant than in the SHANK3 WT protein and SHANK3 L270M mutant, as depicted in (**Figures 7.7D**, **7.5D**, and **7.6D,** respectively). Conversely, the Linker domain showed no significant differences between the SHANK3 WT protein, SHANK3 L270M, and SHANK3 P141A mutants, as illustrated in (**Figures 7.5C**, **7.6C**, and **7.7C**).

Our findings indicated that the SHANK3 WT protein has a heightened level of molecular interactions within the SPN and ARR regions, linking to the overall stability of the protein and maintaining a closed conformation, as shown previously in (**Figure 7.4A**). Conversely, the SHANK3 P141A mutant knocked down the intramolecular connections between SPN and ARR, consequently significantly opening up the distance between SPN and ARR regions, as previously depicted in (**Figure 7.4C**). Numerous investigations have been initiated to unravel the functional importance of the intramolecular connections between SPN and ARR [28] and their implications in the pathogenesis of ASD.

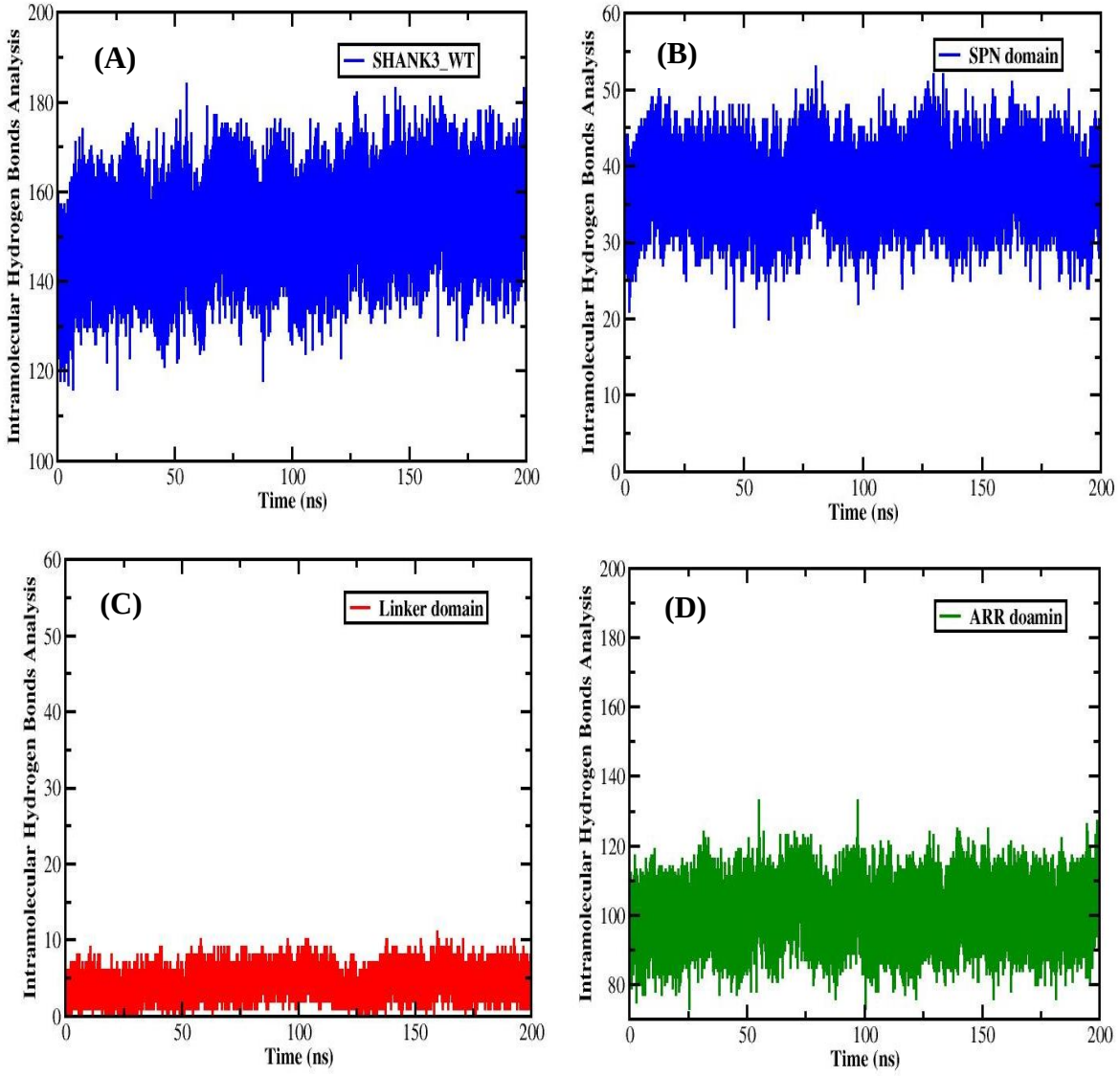

Figure 7.5 *The intramolecular hydrogen bonds analysis, (**A**) SHANK3 WT protein, (**B**) SPN domain, (**C**) WT Linker domain, (**D**) WT ARR domain.*

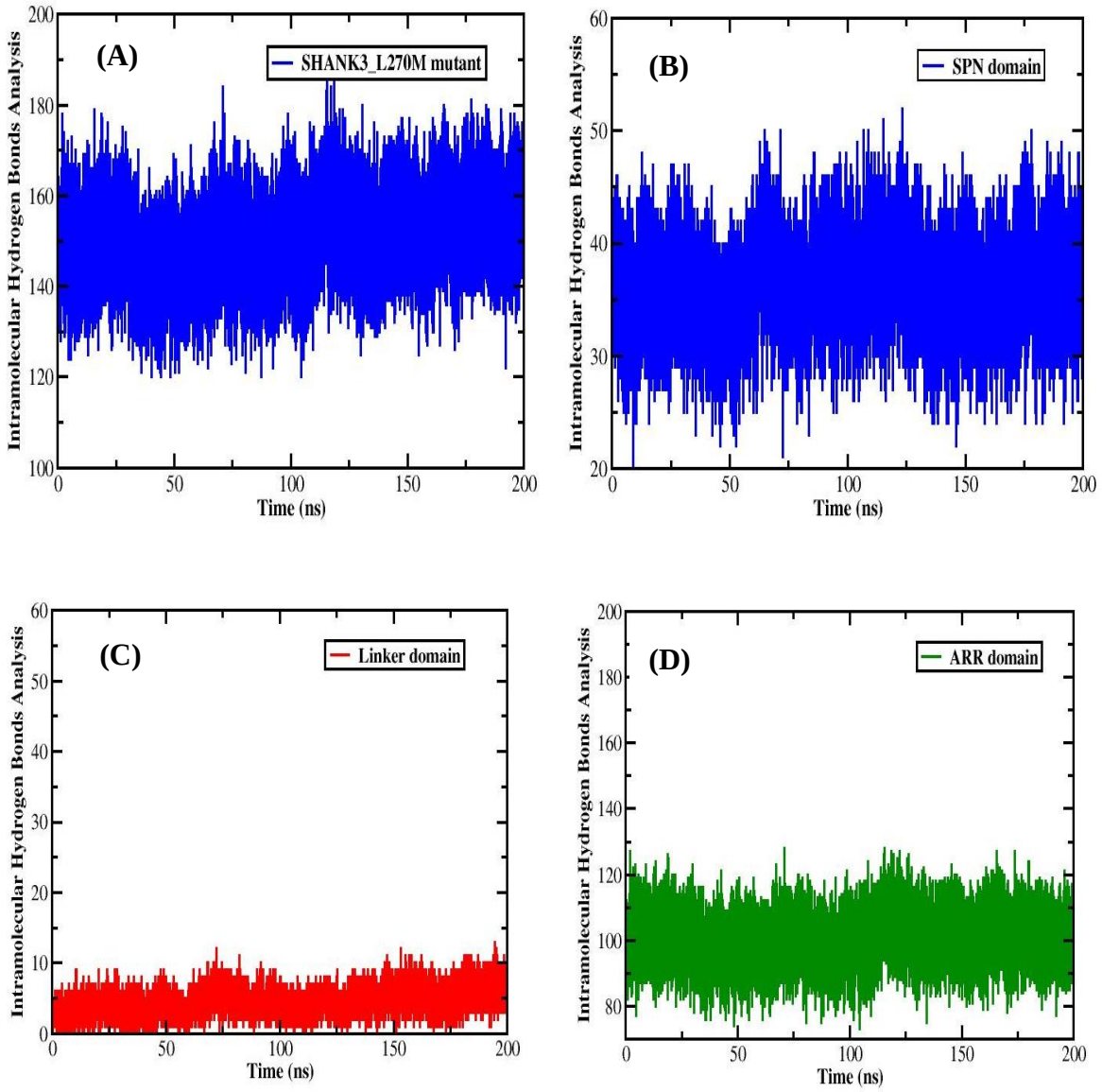

Figure 7.6 *The intramolecular hydrogen bonds analysis, (**A**) SHANK3 L270M mutant, (**B**) SPN domain, (**C**) WT Linker domain, (**D**) WT ARR domain.*

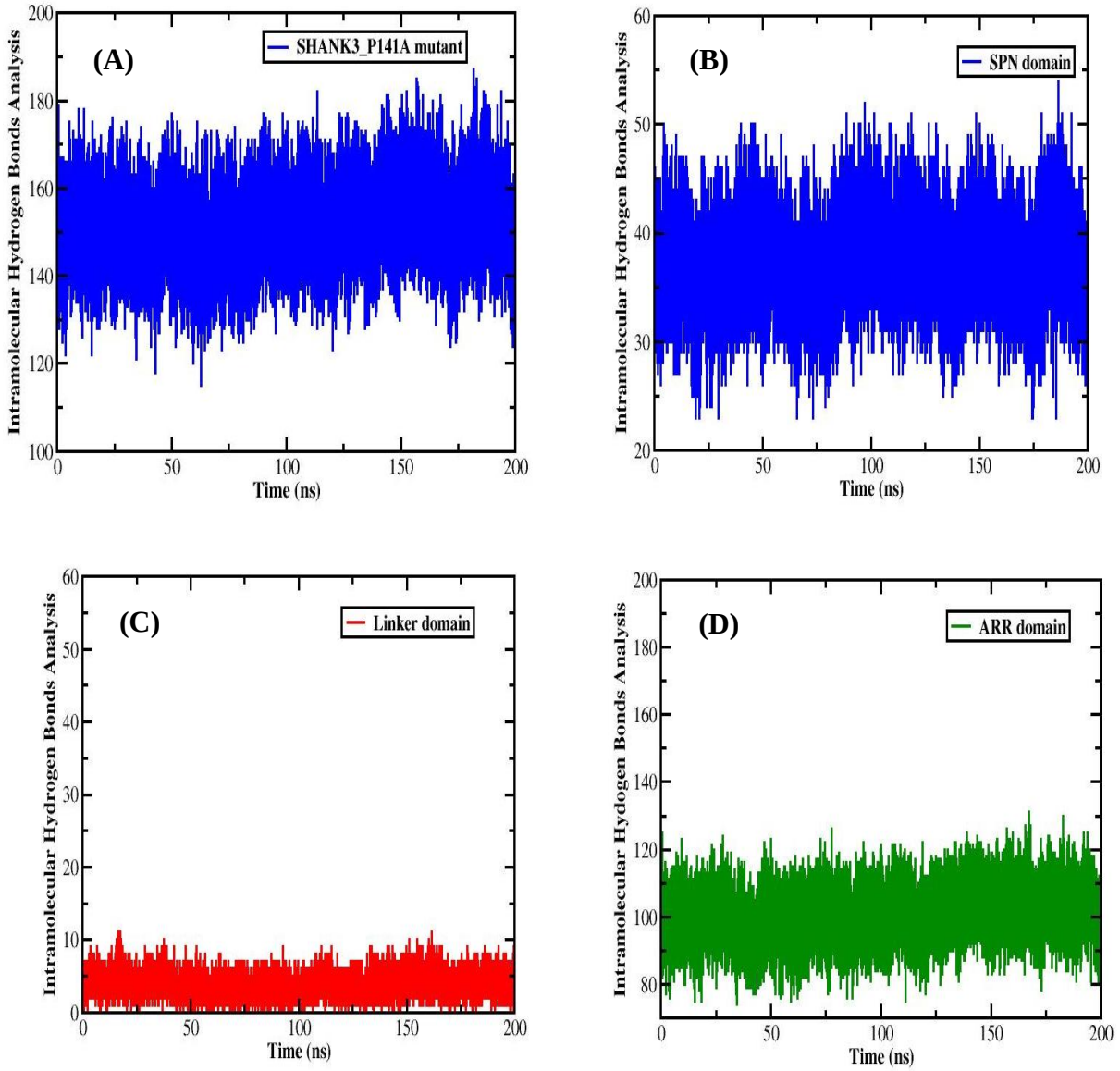

Figure 7.7 *The intramolecular hydrogen bonds analysis, (**A**) SHANK3 P141A mutant, (**B**) SPN domain, (**C**) WT Linker domain, (**D**) WT ARR domain.*

Recent reports have highlighted the involvement of the linker domain connecting both regions, along with a segment of the SPN, in establishing a binding surface for αCaMKII. This binding occurs in its inactive state, non-phosphorylated, and requires a closed configuration of the SPN-ARR tandem [13, 29]. Consequently, disrupting the intramolecular interactions between SPN and ARR regions may induce a conformational change in the Linker domain, resulting in reduced affinity to αCaMKII. In agreement with previously reported results [13, 29], our findings, as seen from (**Figures 7.8A**, **7.9A**, and **Table 7.1**), indicated that the interaction between the SHANK3 WT protein and

αCaMKII exhibits higher affinity in comparison to those predicted for the SHANK3 P141A mutant with αCaMKII, as illustrated in (**Figures 7.8C**, **7.9C**, and **Table 7.3**). Unlike that, the SHANK3 L270M mutant has exhibited a lower affinity, as depicted in (**Figures 7.8B**, **7.9B**, and **Table 7.2**). Hence, a plausible conjecture regarding the SHANK3 L270M mutation arises from its location within the ARR domain, which does not constitute a binding site for αCaMKII.

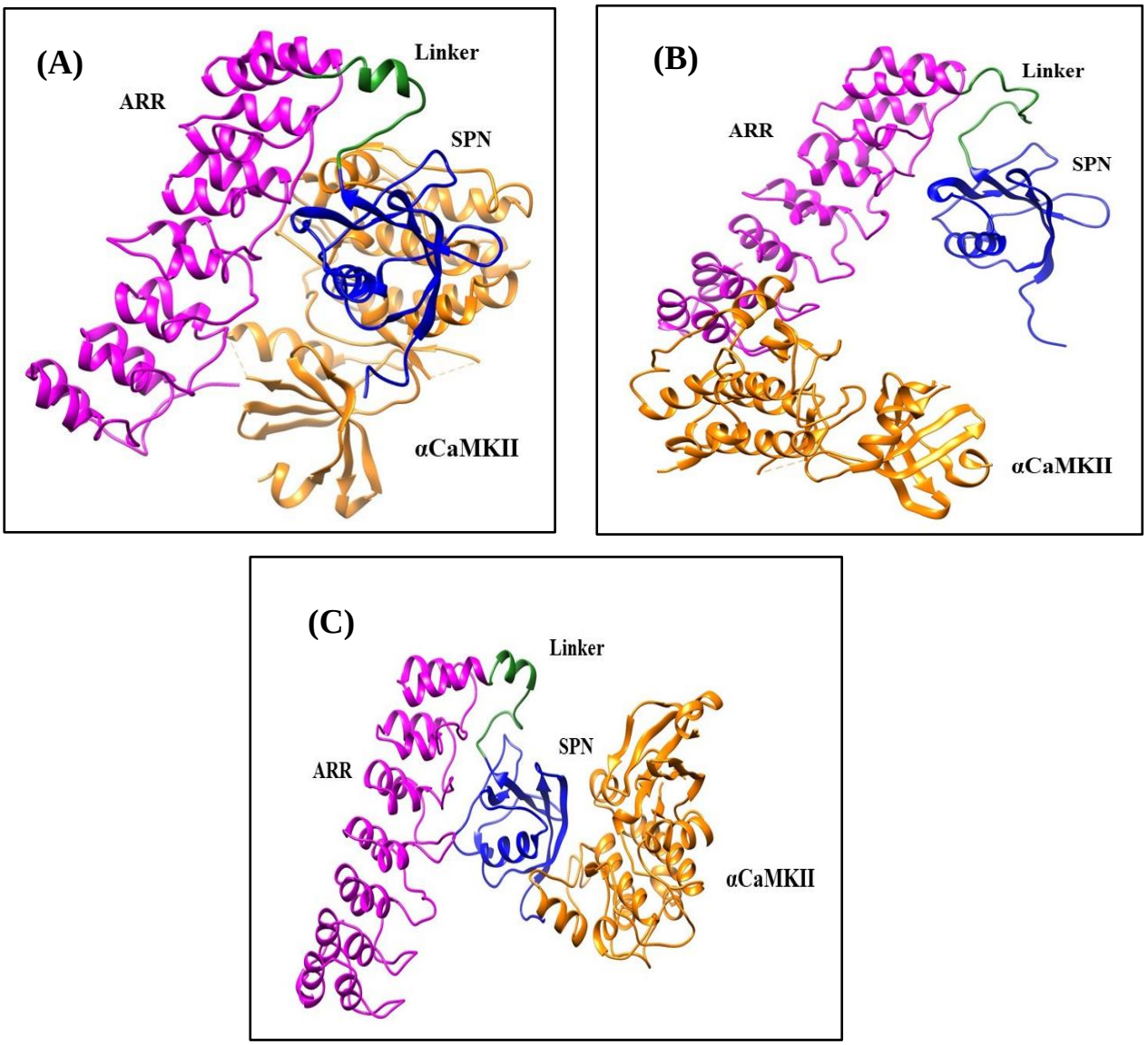

Figure 7.8 *The docking interaction between* ***(A)*** *SHANK3 WT protein and αCaMKII,* ***(B)*** *SHANK3 P141A mutant and αCaMKII,* ***(C)*** *SHANK3 L270M protein and αCaMKII.*

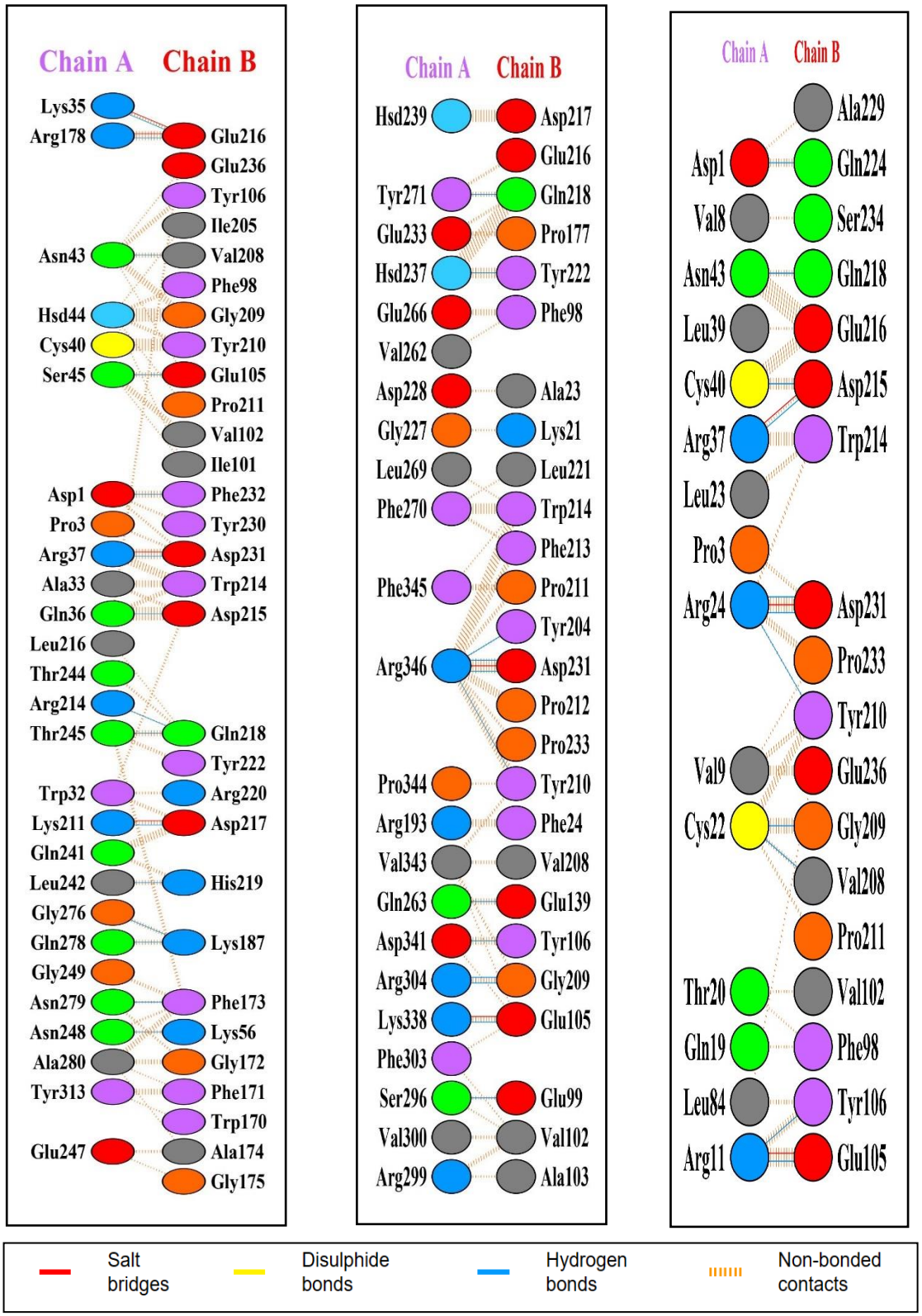

Figure 7.9 *The interactions between* ***(A)*** *SHANK3 WT protein (chain A) and αCaMKII (chain B),* ***(B)*** *SHANK3 P141A mutant (chain A) with αCaMKII (chain B),* ***(C)*** *SHANK3 L270M mutant (chain A) with αCaMKII (chain B).*

Table 7.1 The interface statistics of the SHANK3 WT protein with αCaMKII protein

Chain	No. of interface residues	Interface area (A^2)	No. of salt bridges	No. of disulphide bonds	No. of hydrogen bonds	No. of non-bonded contacts
A (WT)	27	1471	4	-	15	203
B (αCaMKII)	30	1450				

Table 7.2 The interface statistics of the SHANK3 P141A mutant with αCaMKII protein

Chain	No. of interface residues	Interface area (A^2)	No. of salt bridges	No. of disulphide bonds	No. of hydrogen bonds	No. of non-bonded contacts
A (P141A)	23	1238	2	-	12	146
B (αCaMKII)	26	1189				

Table 7.3 The interface statistics of the SHANK3 L270M mutant with αCaMKII protein

Chain	No. of interface residues	Interface area (A^2)	No. of salt bridges	No. of disulphide bonds	No. of hydrogen bonds	No. of non-bonded contacts
A (L270M)	15	872	3	-	11	116
B (αCaMKII)	18	850				

Besides, it should be noted that the distinctive interaction between αCaMKII and SHANK3 plays a pivotal role in instigating a specialized long-range signaling pathway from the plasma cell membrane to the nucleus, and this is true specifically for L-type calcium channels (LTCCs). This signaling mechanism is imperative for inducing activity-dependent alterations in neuronal gene transcription during the processes of memory and learning [30]. It was previously reported in the literature that the disruption of αCaMKII activity emerges as a prevalent process, generating modifications to the structure of glutamatergic and plasticity neuron function, contributing to the pathogenesis of neurological disorders [31].

Conversely, prior research indicates that intramolecular interaction prevents α-Fodrin to access its location on the ARR domain in SHANK3 WT, while SHANK3 P141A significantly boosts the connecting of α-Fodrin to SHANK3 [32]. Considering our findings, which indicated that SHANK3 P141A disrupts the connections between SPN-ARR domains, as well as docking results revealed heightened interactions between α-Fodrin and SHANK3 P141A mutant and SHANK3 L720M mutant (**Tables 7.4** and **7.5**) than SHANK3 WT (**Table 5.3**). Our results aligned with previous study demonstrated that SHANK3 P141A significantly boosts the connecting of α-Fodrin to SHANK3 [13]. One may indicate a potential scenario in which the open conformation facilitates α-Fodrin binding, increases actin linkage, and enhances integrin activation. Taken together, these mutants might change the flexible conformation of SHANK3, leading to an impairment of the capacity to coordinate cytoskeletal aggregation and signaling dysregulation. The physiological activity of the SHANK3-actin connection influences dendritic protrusion morphology in neuron cells and ASD-related characteristics *in vivo* [33]. Notably, SHANK3 loss-of-function mutations have been associated with neurodevelopmental diseases such as ASD [34].

Table 7.4 The interface statistics of the SHANK3 P141A mutant with α-Fodrin protein

Chain	No. of interface residues	Interface area (A^2)	No. of salt bridges	No. of disulphide bonds	No. of hydrogen bonds	No. of non-bonded contacts
A (SHANK3 P141A)	17	735	4	-	13	115
B (α-Fodrin)	16	749				

Table 7.5 The interface statistics of the SHANK3 L270M mutant with α-Fodrin protein

Chain	No. of interface residues	Interface area (A^2)	No. of salt bridges	No. of disulphide bonds	No. of hydrogen bonds	No. of non-bonded contacts
A (SHANK3 L270M)	17	770	3	-	9	114
B (α-Fodrin)	14	751				

7.4.6. Intermolecular hydrogen bonds analysis

The interaction between the SPN and ARR domains was investigated through hydrogen bonds. The findings revealed that the SHANK3 WT protein exhibited more hydrogen bonds than the SHANK3 L270M mutant and SHANK3 P141A mutant, as shown in (**Figures. 7.10A**, **7.10B**, and **7.10C**, respectively), indicating more stability.

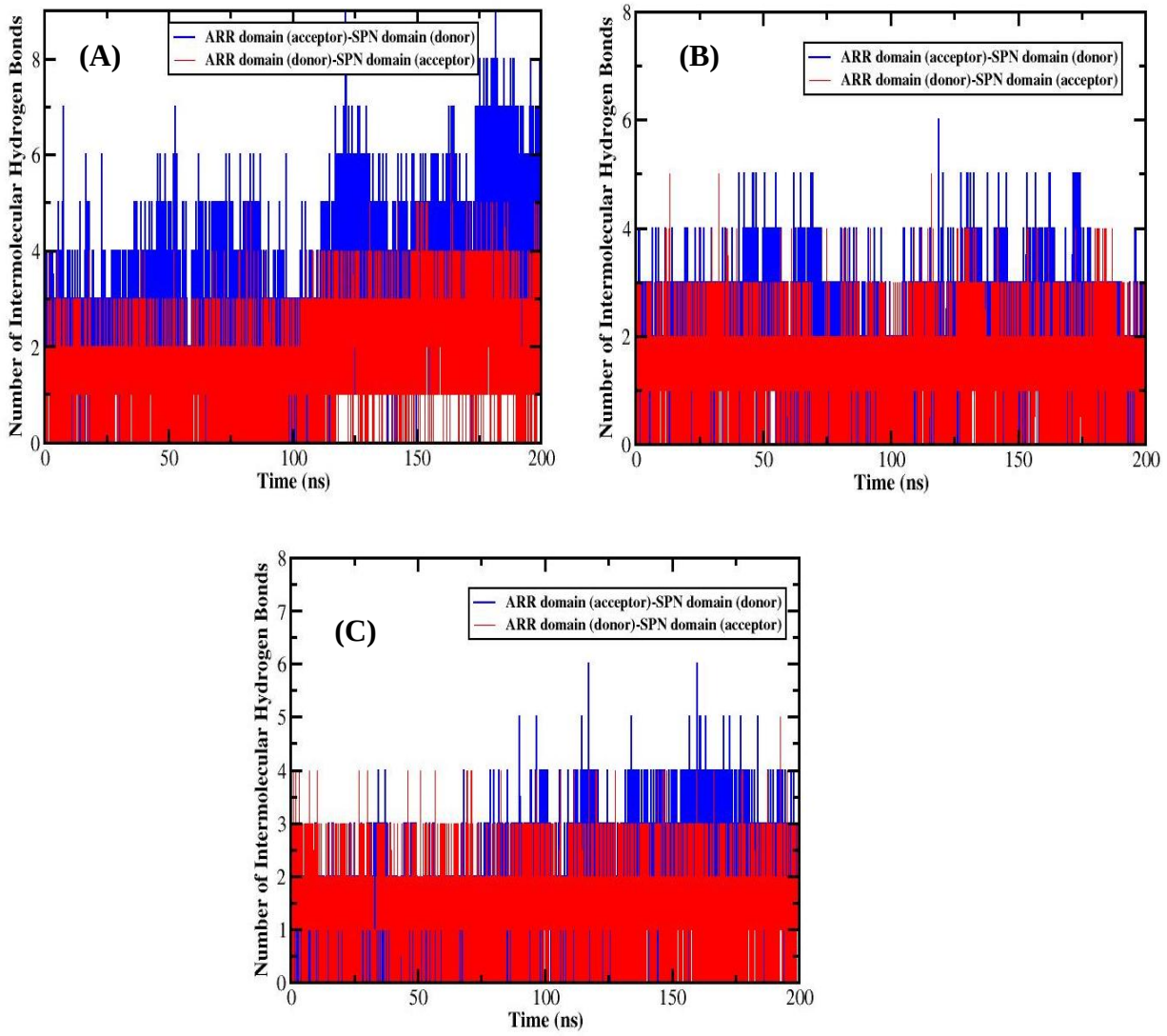

Figure 7.10 *The number of H-bonds between SPN-ARR domains for 200 ns MD simulation, (**A**) SHANK3 WT, (**B**) SHANK3 L270M mutant, (**C**) SHANK3 P141A mutant.*

7.4.7. Secondary structure analysis

The Kabsch and Sander algorithm [35] within the DSSP program was employed for secondary structure analysis of the three structures of SHANK3 WT protein and the two mutants, SHANK3 L270M and P141A. The plots depicting the results for the secondary structure analysis for the SHANK3 WT protein are presented in (**Figure 7.11A**) and the SHANK3 L270M mutant, as shown in (**Figure 7.12A**), as well as for the SHANK3 P141A mutant (**Figure 7.13A**). The graphics represent the variability of secondary structure across each residue as an indication of frame numbers. In addition, the proportion content of individual secondary structures in the SHANK3 WT protein,

SHANK3 L270M, and SHANK3 P141A mutants was determined over their respective average structures generated in 200 ns MD simulations, which were carried out by using YASARA software [36]. The findings indicate that the SHANK3 L270M mutant and SHANK3 P141A mutant exhibit a higher helical content than the SHANK3 WT protein, as shown in (**Table 7.6**). We conducted an assessment of the secondary structure probability assumed by the SHANK3 WT and two variants, namely SHANK3 L270M and SHANK3 P141A mutants, employing quantitative measures as a function of residue index, as delineated in (**Figure 7.11B**) for SHANK3 WT protein. (**Figure 7.12B**) presents the SHANK3 L270M mutant, as well as SHANK3 P141A mutant as shown in (**Figure 7.13B**).

Table 7.6 Secondary structure content of the SHANK3 WT protein and two mutant forms, SHANK3 L270M and SHANK3 P141A, showing the secondary contents of α-helix, β-sheets, Turns, 3_{10}-helix, Coils, and Pi

COMPLEX	α-helix %	β-sheet %	turn %	Pi-helix %	3_{-10} helix %	Coil %
WT	40.8	6.9	17.3	0	0	35
L270M	43.4	7.8	19.4	0	0	29.5
P141A	44.1	10	16.8	0	0	30.1

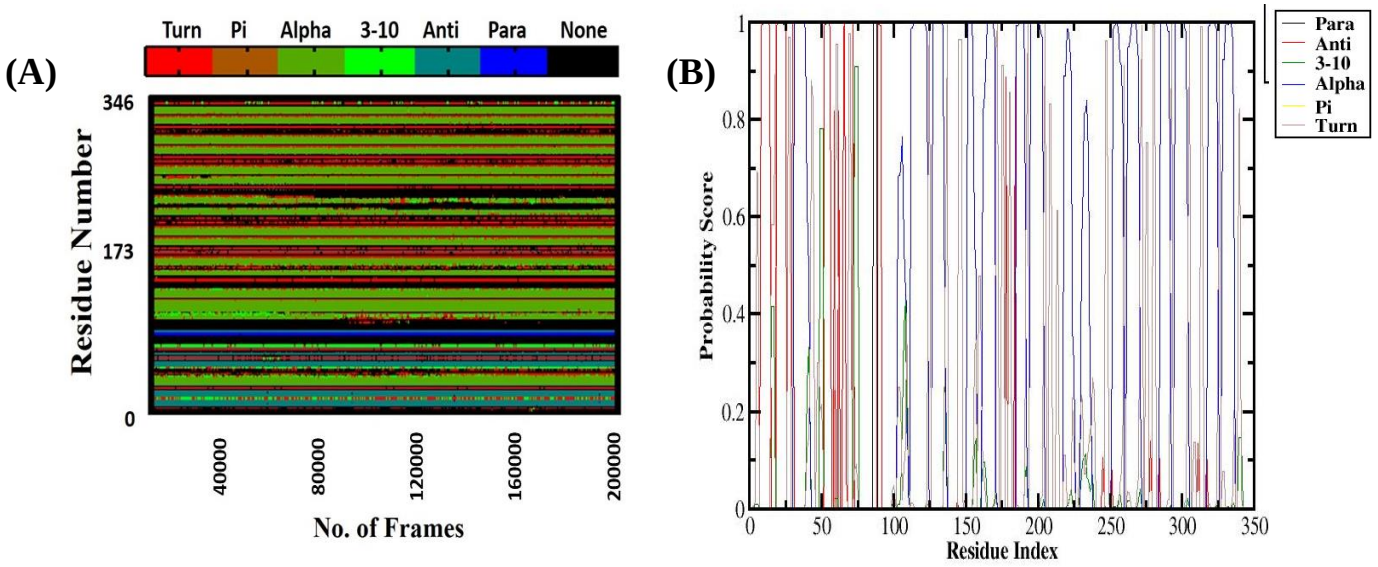

Figure 7.11 *Secondary structure analysis (**A**) SHANK3 WT Protein. Secondary structure probability score of residue index: (**B**) SHANK3 WT protein.*

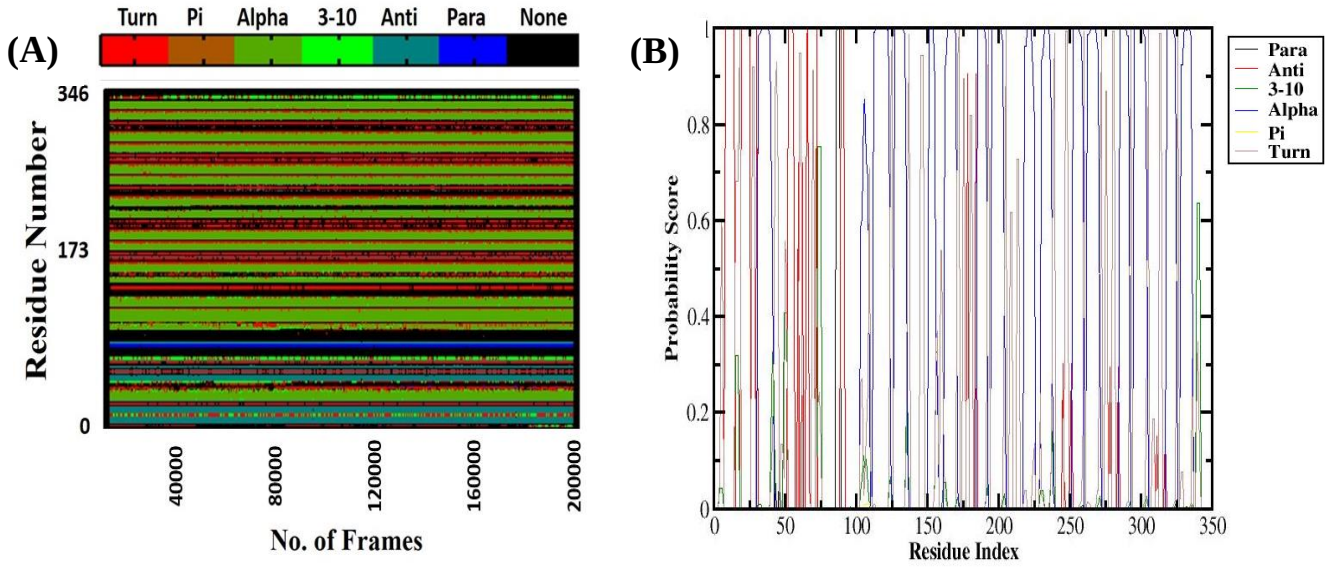

Figure 7.12 *Secondary structure analysis (**A**) SHANK3 L270M mutant. Secondary structure probability score of residue index: (**B**) SHANK3 L270M mutant.*

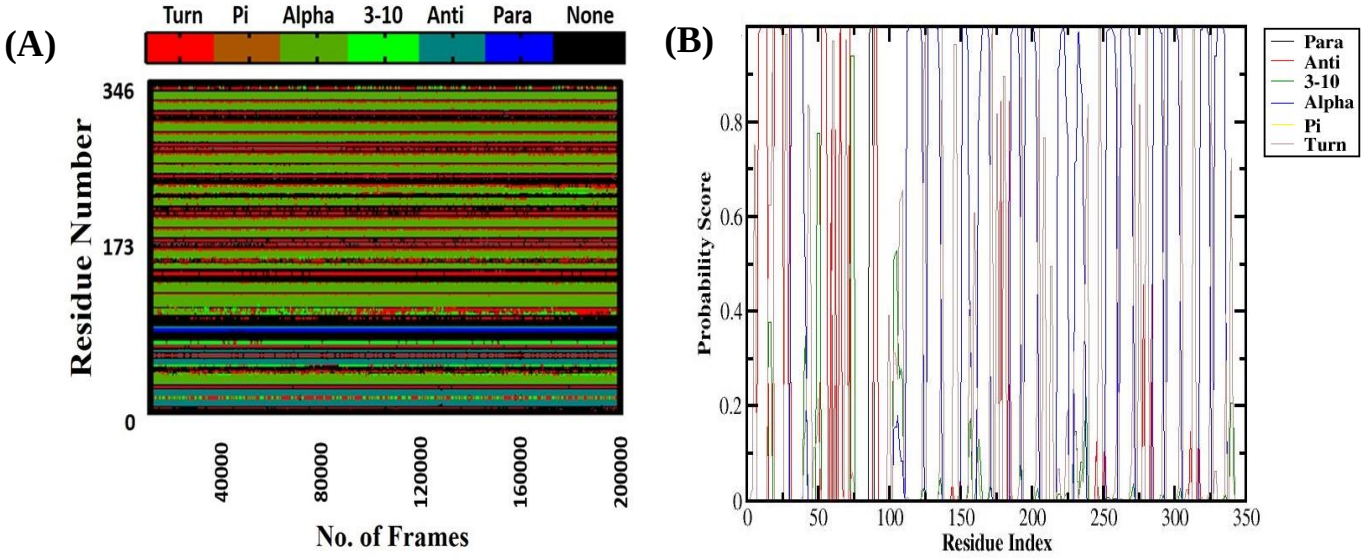

Figure 7.13 *Secondary structure analysis (**A**) SHANK3 P141A mutant. Secondary structure probability score of residue index: (**B**) SHANK3 P141A mutant.*

7.5. Conclusion

In conclusion, our study extensively investigated the role of SHANK3 P141A and SHANK3 L270M mutants within the SHANK3 gene, particularly in the N-terminal region. The SHANK3 P141A mutant exhibited a significant impact, hindering the stabilization and folding of SHANK3, as well as disrupting intramolecular interactions between SPN and ARR, influencing its binding with αCaMKII and α-Fodrin as a protein patners, which will have a significant impact on synaptic functionality and might play a potential role in ASD. In contrast, the SHANK3 L270M mutant exhibited a moderate stability and lesser intramolecular hydrogen bonding when compared to the SHANK3 WT mutant. These findings emphasize the intricate dynamics of SHANK3 mutations and suggest that their potential contributions to neurodevelopmental disorders such as ASD, warranting further computational and experimental investigations to elucidate their precise role in ASD pathogenesis.

References

[1] Zeidan, J., Fombonne, E., Scorah, J., Ibrahim, A., Durkin, M. S., Saxena, S., Yusuf, A., Shih, A. and Elsabbagh, M. Global prevalence of autism: A systematic review update. *Autism research,* 15: 778-790, 2022. https://doi.org/10.1002/aur.2696

[2] Ghafouri-Fard, S., Pourtavakoli, A., Hussen, B. M., Taheri, M. and Ayatollahi, S. A. A Review on the Role of Genetic Mutations in the Autism Spectrum Disorder. *Molecular Neurobiology,* 60: 5256–5272, 2023. https://doi.org/10.1007/s12035-023-03405-9

[3] Alonso-Gonzalez, A., Rodriguez-Fontenla, C. and Carracedo, A. De novo mutations (DNMs) in autism spectrum disorder (ASD): Pathway and network analysis. *Front. genet.,* 9: 1-14, 2018. https://doi.org/10.3389/fgene.2018.00406

[4] Molloy, C. J., Cooke, J., Gatford, N. J., Rivera-Olvera, A., Avazzadeh, S., Homberg, J. R., Grandjean, J., Fernandes, C., Shen, S. and Loth, E. Bridging the translational gap: what can synaptopathies tell us about autism? *Frontiers in Molecular Neuroscience,* 16: 1-20, 2023. https://doi.org/10.3389/fnmol.2023.1191323

[5] Monteiro, P. and Feng, G. SHANK proteins: roles at the synapse and in autism spectrum disorder. *Nat. Rev. Neurosci.,* 18: 147-157, 2017. https://doi.org/10.1038/nrn.2016.183

[6] Ivashko-Pachima, Y., Ganaiem, M., Ben-Horin-Hazak, I., Lobyntseva, A., Bellaiche, N., Fischer, I., Levy, G., Sragovich, S., Karmon, G. and Giladi, E. SH3-and actin-binding domains connect ADNP and SHANK3, revealing a fundamental shared mechanism underlying autism. *Molecular psychiatry,* 27: 3316-3327, 2022.

[7] Sheng, M. and Kim, E. The Shank family of scaffold proteins. *J. Cell Sci.,* 113: 1851-1856, 2000. https://doi.org/10.1242/jcs.113.11.1851

[8] Lilja, J., Zacharchenko, T., Georgiadou, M., Jacquemet, G., Franceschi, N. D., Peuhu, E., Hamidi, H., Pouwels, J., Martens, V. and Nia, F. H. SHANK proteins limit integrin activation by directly interacting with Rap1 and R-Ras. *Nature cell biology,* 19: 292-305, 2017. https://doi.org/10.1038/ncb3487

[9] Cai, Q., Hosokawa, T., Zeng, M., Hayashi, Y. and Zhang, M. Shank3 binds to and stabilizes the active form of Rap1 and HRas GTPases via Its NTD-ANK tandem with distinct mechanisms. *Structure,* 28: 290-300. e4, 2020. https://doi.org/10.1016/j.str.2019.11.018

[10] Peça, J., Feliciano, C., Ting, J. T., Wang, W., Wells, M. F., Venkatraman, T. N., Lascola, C. D., Fu, Z. and Feng, G. Shank3 mutant mice display autistic-like behaviours

and striatal dysfunction. *Nature*, 472: 437-442, 2011. https://doi.org/10.1038/nature09965

[11] Barak, B. and Feng, G. Neurobiology of social behavior abnormalities in autism and Williams syndrome. *Nature neuroscience*, 19: 647-655, 2016. https://doi.org/10.1038/nn.4276

[12] Owji, H., Eslami, M., Nezafat, N. and Ghasemi, Y. In Silico Elucidation of Deleterious Non-synonymous SNPs in SHANK3, the Autism Spectrum Disorder Gene. *Journal of Molecular Neuroscience*, 70: 1649-1667, 2020. https://doi.org/10.1007/s12031-020-01552-5

[13] Woike, D., Wang, E., Tibbe, D., Hassani Nia, F., Failla, A. V., Kibæk, M., Overgård, T. M., Larsen, M. J., Fagerberg, C. R. and Barsukov, I. Mutations affecting the N-terminal domains of SHANK3 point to different pathomechanisms in neurodevelopmental disorders. *Scientific Reports*, 12: 902, 2022. https://doi.org/10.1038/s41598-021-04723-5

[14] Boccuto, L., Lauri, M., Sarasua, S. M., Skinner, C. D., Buccella, D., Dwivedi, A., Orteschi, D., Collins, J. S., Zollino, M. and Visconti, P. Prevalence of SHANK3 variants in patients with different subtypes of autism spectrum disorders. *European Journal of Human Genetics*, 21: 310-316, 2013. https://doi.org/10.1038/ejhg.2012.175

[15] Moessner, R., Marshall, C. R., Sutcliffe, J. S., Skaug, J., Pinto, D., Vincent, J., Zwaigenbaum, L., Fernandez, B., Roberts, W. and Szatmari, P. Contribution of SHANK3 mutations to autism spectrum disorder. *The American Journal of Human Genetics*, 81: 1289-1297, 2007. https://doi.org/10.1086/522590

[16] Durand, C. M., Perroy, J., Loll, F., Perrais, D., Fagni, L., Bourgeron, T., Montcouquiol, M. and Sans, N. SHANK3 mutations identified in autism lead to modification of dendritic spine morphology via an actin-dependent mechanism. *Molecular psychiatry*, 17: 71-84, 2012. https://doi.org/10.1038/mp.2011.57

[17] Berman, H. M., Westbrook, J., Feng, Z., Gilliland, G., Bhat, T. N., Weissig, H., Shindyalov, I. N. and Bourne, P. E. The Protein Data Bank. *Nucleic acids research*, 28: 235-242, 2000. https://doi.org/10.1093/nar/28.1.235

[18] Rose, P. W., Prlić, A., Bi, C., Bluhm, W. F., Christie, C. H., Dutta, S., Green, R. K., Goodsell, D. S., Westbrook, J. D. and Woo, J. The RCSB Protein Data Bank: views of structural biology for basic and applied research and education. *Nucleic Acids Res.*, 43: D345-D356, 2015. https://doi.org/10.1093/nar/gku1214

[19] Pettersen, E. F., Goddard, T. D., Huang, C. C., Couch, G. S., Greenblatt, D. M., Meng, E. C. and Ferrin, T. E. UCSF Chimera—a visualization system for exploratory research and analysis. *J. Comput. Chem.*, 25: 1605-1612, 2004. https://doi.org/10.1002/jcc.20084

[20] Henriques, J., Cragnell, C. and Skepo, M. Molecular dynamics simulations of intrinsically disordered proteins: force field evaluation and comparison with experiment. *J. Chem. Theory Comput.*, 11: 3420-3431, 2015. https://doi.org/10.1021/ct501178z

[21] Jorgensen, W. L., Chandrasekhar, J., Madura, J. D., Impey, R. W. and Klein, M. L. Comparison of simple potential functions for simulating liquid water. *The Journal of chemical physics*, 79: 926-935, 1983. https://doi.org/10.1063/1.445869

[22] Ryckaert, J.-P., Ciccotti, G. and Berendsen, H. J. Numerical integration of the cartesian equations of motion of a system with constraints: molecular dynamics of n-alkanes. *Journal of computational physics*, 23: 327-341, 1977. https://doi.org/10.1016/0021-9991(77)90098-5

[23] Salomon-Ferrer, R., Gotz, A. W., Poole, D., Le Grand, S. and Walker, R. C. Routine microsecond molecular dynamics simulations with AMBER on GPUs. 2. Explicit solvent particle mesh Ewald. *J. Chem. Theory Comput.*, 9: 3878-3888, 2013. https://doi.org/10.1021/ct400314y

[24] Berendsen, H. J., Postma, J. v., Van Gunsteren, W. F., DiNola, A. and Haak, J. R. Molecular dynamics with coupling to an external bath. *J. Chem. Phys.*, 81: 3684-3690, 1984. https://doi.org/10.1063/1.448118

[25] Knapp, B., Frantal, S., Cibena, M., Schreiner, W. and Bauer, P. Is an intuitive convergence definition of molecular dynamics simulations solely based on the root mean square deviation possible? *J. Comput. Biol.*, 18: 997-1005, 2011. https://doi.org/10.1089/cmb.2010.0237

[26] Falsafi-Zadeh, S., Karimi, Z. and Galehdari, H. VMD DisRg: New User-Friendly Implement for calculation distance and radius of gyration in VMD program. *Bioinformation*, 8: 341-343, 2012. https://doi.org/10.6026/97320630008341

[27] Adegbola, A., Lutz, R., Nikkola, E., Strom, S. P., Picker, J. and Wynshaw-Boris, A. Disruption of CTNND2, encoding delta-catenin, causes a penetrant attention deficit disorder and myopia. *Hum. Genet. Genom. Adv.*, 1: 1-12, 2020. https://doi.org/10.1016/j.xhgg.2020.100007

[28] Woike, D., Tibbe, D., Hassani Nia, F., Martens, V., Wang, E., Barsukov, I. and Kreienkamp, H.-J. The Shank/ProSAP N-terminal (SPN) domain of Shank3 regulates targeting to postsynaptic sites and postsynaptic signalling. *bioRxiv,* 1-21, 2023. https://doi.org/10.1101/2023.04.28.538665

[29] Cai, Q., Zeng, M., Wu, X., Wu, H., Zhan, Y., Tian, R. and Zhang, M. CaMKIIα-driven, phosphatase-checked postsynaptic plasticity via phase separation. *Cell Research,* 31: 37-51, 2021. https://doi.org/10.1038/s41422-020-00439-9

[30] Perfitt, T. L., Wang, X., Dickerson, M. T., Stephenson, J. R., Nakagawa, T., Jacobson, D. A. and Colbran, R. J. Neuronal L-type calcium channel signaling to the nucleus requires a novel CaMKIIα-Shank3 interaction. *J. Neurosci.,* 40: 2000-2014, 2020. https://doi.org/10.1523/JNEUROSCI.0893-19.2020

[31] Robison, A. Emerging role of CaMKII in neuropsychiatric disease. *Trends Neurosci.,* 37: 653-662, 2014. https://doi.org/10.1016/j.tins.2014.07.001

[32] Mameza, M. G., Dvoretskova, E., Bamann, M., Hönck, H.-H., Güler, T., Boeckers, T. M., Schoen, M., Verpelli, C., Sala, C. and Barsukov, I. SHANK3 gene mutations associated with autism facilitate ligand binding to the Shank3 ankyrin repeat region. *Journal of Biological Chemistry,* 288: 26697-26708, 2013. https://doi.org/10.1074/jbc.M112.424747

[33] Salomaa, S. I., Miihkinen, M., Kremneva, E., Paatero, I., Lilja, J., Jacquemet, G., Vuorio, J., Antenucci, L., Kogan, K. and Nia, F. H. SHANK3 conformation regulates direct actin binding and crosstalk with Rap1 signaling. *Current Biology,* 31: 4956-4970, 2021. https://doi.org/10.1016/j.cub.2021.09.022

[34] Bucher, M., Niebling, S., Han, Y., Molodenskiy, D., Hassani Nia, F., Kreienkamp, H.-J., Svergun, D., Kim, E., Kostyukova, A. S. and Kreutz, M. R. Autism-associated SHANK3 missense point mutations impact conformational fluctuations and protein turnover at synapses. *Elife*, 10: 1-31, 2021. https://doi.org/10.7554/eLife.66165

[35] Kabsch, W. and Sander, C. Dictionary of protein secondary structure: pattern recognition of hydrogen-bonded and geometrical features. *Biopolymers: Original Research on Biomolecules*, 22: 2577-2637, 1983. https://doi.org/10.1002/bip.360221211

[36] Krieger, E., Koraimann, G. and Vriend, G. Increasing the precision of comparative models with YASARA NOVA—a self-parameterizing force field. *Proteins: Struct. Funct. Genet.*, 47: 393-402, 2002. https://doi.org/10.1002/prot.10104